An experimental and modeling study of the low- and high-temperature oxidation of cyclohexane

Zeynep Serinyel, Olivier Herbinet, Ophélie Frottier, Patricia Dirrenberger, Valérie Warth, Pierre Alexandre Glaude, Frédérique Battin-Leclerc

An experimental and modeling study of the low- and high-temperature oxidation of cyclohexane

Zeynep Serinyel, Olivier Herbinet, Ophélie Frottier, Patricia Dirrenberger, Valérie Warth, Pierre Alexandre Glaude, Frédérique Battin-Leclerc

Laboratoire Réactions et Génie des Procédés, UMR 7274 CNRS, Université de Lorraine, 1 rue Grandville, 54001 Nancy, France

Abstract

The experimental study of the oxidation of cyclohexane has been performed in a jet-stirred reactor at temperatures ranging from 500 to 1100 K (low- and intermediate temperature zones including the negative temperature-coefficient area), at a residence time of 2 s and for dilute mixtures with equivalence ratios of 0.5, 1, and 2. Experiments were carried out at quasi-atmospheric pressure (1.07 bar). The fuel and reaction product mole fractions were measured using online gas chromatography. A total of 34 reaction products have been detected and quantified in this study. Typical reaction products formed in the low-temperature oxidation of cyclohexane include cyclic ethers (1,2-epoxycyclohexane and 1,4-epoxycyclohexane), 5-hexenal (formed from the rapid decomposition of 1,3-epoxycyclohexane), cyclohexanone, and cyclohexene, as well as benzene and phenol. Cyclohexane displays high low-temperature reactivity with well-marked negative temperature-coefficient (NTC) behavior at equivalence ratios 0.5 and 1. The fuel-rich system (ϕ = 2) is much less reactive in the same region and exhibits no NTC. To the best of our knowledge, this is the first jet-stirred reactor study to report NTC in cyclohexane oxidation. Laminar burning velocities were also measured by the heated burner method at initial gas temperatures of 298, 358, and 398 K and at 1 atm. The laminar burning velocity values peak at ϕ = 1.1 and are measured as 40 and 63.1 cm/s for T_i = 298 and 398 K, respectively. An updated detailed chemical kinetic model including low-temperature pathways was used to simulate the present (jet-stirred reactor and laminar burning velocity) and literature experimental (laminar burning velocity, rapid compression machine, and shock tube ignition delay times) data. Reasonable agreement is observed with most of the products observed in our reactor, as well as the literature experimental data considered in this paper.

Keywords: Jet-stirred reactor; Cyclohexane; Low-temperature oxidation; Laminar burning velocity

1. Introduction

Cyclic alkanes are an important part of the composition of gasoline, diesel, and jet fuels; in fact, they can represent at least 30% of diesel fuel [1]. Cyclohexane is a simple model cycloalkane used as a surrogate to represent the cyclic alkanes in a real fuel.

Cyclohexane has been the subject of interest to many researchers and has been more widely investigated than alkylated naphthenes in terms of combustion properties. Table 1 summarizes the experimental studies of cyclohexane in the literature since 1965. The earliest studies of cyclohexane oxidation were performed by Zeelenberg and DeBruijn [2] and Bonner and Tipper [3], who studied cyclohexane oxidation in static reaction vessels. Klai and Baronnet performed a study in a static reactor at 653 K and 4.7 kPa [4] and [5]. Another early study was performed by the Walker group [6], conducted in a static vessel at 753 K by adding cyclohexane into H_2–O_2 mixtures; they later studied the reaction between HO2 radicals and cyclohexane [7]. Both studies reported a product analysis. Hong et al. [8], Daley et al. [9], and Sirjean et al. [10] studied cyclohexane oxidation behind reflected shock waves at high temperatures (850 K < T < 1500 K) for lean, stoichiometric, and rich mixtures of cyclohexane in argon or air and at pressures ranging from 1.5 to 50 atm. Lemaire et al. [11] and more recently Vranckx et al. [12] measured cyclohexane ignition delay times in rapid compression machines in temperature ranges covering the NTC area and at compressed gas pressures ranging from 7 to 40 bar. The former RCM study [11] also reports the evolution of intermediate products using gas chromatography and mass spectroscopy, including benzene. Wang et al. [13] studied cyclohexane pyrolysis in a plug flow reactor under low-pressure conditions (40 mbar) from 950 to 1520 K. The first jet-stirred reactor study of cyclohexane oxidation was carried out by Voisin et al. [14] between 750 and 1100 K at 10 atm; they also proposed a chemical kinetic mechanism to represent their data. El-Bakali et al. [15] later extended this study to lower pressures and shorter residence times, and they also revised the kinetic mechanism and extended its domain of validation. Note that no NTC regime of cyclohexane could be observed in either of the studies, due to the temperature range. Laminar burning velocities of cyclohexane were measured by groups at Princeton [16] and [17] and USC [18] between 1 and 20 atm. Given the sooting propensity of cyclohexane, benzene/soot formation has also been investigated by various groups [19], [20], [21] and [22]. Yang and Boehman [23] investigated cyclohexane oxidation at low/intermediate temperatures in a CFR engine and analyzed exhaust products, and they observed negative temperature behavior.

Table 1. Experimental investigations of cyclohexane in literature.

Experimental device	T (K)	P	ϕ and mixture conditions	Ref.
Static vessel / Flow tube	533 – 673	0.067–0.13 bar	Cyclohexane/air (1:2 to 2:1)	[2]
Static vessel	503 – 623	0.027–0.27 bar	Cyclohexane/O_2 1:1	[3]
Static vessel	635	0.047 bar	$\phi = 9$	[4-5]
Static vessel	753	0.667 bar	$0.003 < \phi < 0.032$	[6]
Static vessel	673 – 773	P_{tot} = 0.02 bar	$0.9 < \phi < 5.1$	[7]
Shock tube	1300 – 1500	1.5 – 5 atm	ϕ =1.0 and 0.5	[8]
Shock tube	850 – 1380	15 and 50 atm	$\phi = 0.25$, 0.5 and 1.0	[9]
Shock tube	1300 – 1500	7.3 – 9.5 atm	$\phi = 0.25$, 0.5 and 1.0	[10]
Rapid compression machine	600 – 900	7 – 14 bar	$\phi = 1.0$	[11]
Rapid compression machine	680 – 910	12 – 40 bar	$\phi = 0.5$, 1.0 and 2.0	[12]
Plug flow reactor	950 – 1520	40 mbar	pyrolysis	[13]
Jet-stirred reactor	750 – 1100	10 atm	$0.5 < \phi < 1.5$	[14]
Jet-stirred reactor	850 – 1100	1, 2 and 10 atm	$0.5 < \phi < 1.5$	[15]
Laminar burning velocity (spherical flame)	T_i = 353	1, 2, 5 and 10 atm	$0.6 < \phi < 1.6$	[16]
Laminar burning velocity (counter-flow flame)	T_i = 353	1 atm	$0.7 < \phi < 1.5$	[18]
Laminar burning velocity (counter-flow flame)	T_i = 298	1 atm	$0.7 < \phi < 1.7$	[17]
Laminar premixed flat flame	T_{max} = 1950	0.04 bar	$\phi = 1$	[19]
Non-premixed flame (co-flow)	T_{max} = 2000	1 atm	2000 ppm cyclohexane in CH_4/air flame	[20]
Premixed laminar flat flame	T_{max} = 2000	1 atm	$\phi = 2.23$ (C/O ratio = 0.77)	[21]
Premixed laminar flat flame	T_{max} ~ 2200	0.04 bar	$\phi = 2$	[22]
CFR engine	T_{intake} = 393 and 473 T_{max} = 800 and 860	P_{intake} = 1 atm P_{max} = 21.2 – 24.6 bar	$\phi = 0.25$	[23]

Several chemical kinetic mechanisms have also been proposed for cyclohexane oxidation; a mechanism developed by the Orléans group as mentioned above, validated against their oxidation data [14] and [15] above 750 K, and laminar flame speeds [17]. This mechanism is not validated against data taken in the cool flame regime. Granata et al. [24] proposed a detailed mechanism for the oxidation of naphthenes, also validated against low- and high-temperature experimental data

including jet-stirred reactor, RCM, and laminar burning velocities [11], [14], [15] and [17]. Silke et al. [25] proposed a detailed mechanism developed in a hierarchical manner validated against data from Lille [11] and Orléans [14] and [15]. Another mechanism is proposed by the USC group for the combustion of jet-fuel surrogate [26]; however, this mechanism contains only high-temperature reactions and therefore is only validated in the high-temperature domain. The mechanism of Buda et al. [27], later updated by Sirjean and co-workers [28], is automatically generated (using EXGAS package, which will be described in this paper) and includes both low- and high-temperature chemistry for cyclohexane. These mechanisms are also validated against Lille RCM [11], Orléans JSR [14] and [15], and Nancy shock tube [10] data.

The present study mainly aims at investigating both low- and high-temperature oxidation of cyclohexane. For the jet-stirred reactor part of this study, the temperature range is set to 500 K < T < 1100 K in order to cover the whole reactivity range and to be able to analyze different oxidation regimes, including the NTC region. The chemical kinetic mechanism was automatically generated by EXGAS (this will be explained in the coming section) and extended to capture the formation of the stable organic species as listed in Table 2.

Table 2. Quantified stable organic species.

Saturated and unsaturated hydrocabons	methane, acetylene, ethylene, ethane, propane, propadiene, propyne*, allene*, *iso*- and, *1*-butene, 1,3-butadiene, 1,4-pentadiene*
Linear oxygenated species	Formaldehyde, acetaldehyde, methanol, methoxyethylene, acrolein, propanal
Cyclic species	Ethylene oxide, furan*, 3-butenyl-oxirane, cyclopentene, cyclopentadiene, cyclopentanecarboxyaldehyde, benzene, cyclohexene, cyclohexane, toluene*, 5-hexenal, 1,2-epoxycyclohexane, 1,4-epoxycylohexane, cyclohexanone, 2-cyclo-hexen-1-one

*These species were quantified with concentrations below 20 ppm.

2. Experimental method

The experiments were carried out in a jet-stirred reactor for speciation (using gas chromatography) and an adiabatic flat flame burner for the measurement of laminar burning velocities. The experimental conditions are given in Table 3. All experiments were carried out at atmospheric pressure.

Table 3. Experimental conditions.

	Jet-stirred reactor			Flat flame burner
Temperature (K)	500 < *T* < 1100			T_i = 298, 358, 398
Equivalence ratio	ϕ = 0.5, 1.0, 2.0			$0.6 < \phi < 1.6$
Mixture composition	ϕ = 0.5 0.667 % fuel 12 % O_2	ϕ = 1.0 0.667 % fuel 6 % O_2	ϕ = 2.0 0.667 % fuel 3 % O_2	fuel in air

2.1. Jet-stirred reactor experiments

The study of cyclohexane oxidation was performed in a jet-stirred reactor with quantification of species using gas chromatography.

2.1.1. Description of the experimental apparatus

The jet-stirred reactor belongs to the category of continuous stirred-tank reactors [29]. The jet-stirred reactor used in this study was developed following the rules of construction given by Matras and Villermaux [29] and David and Matras [30]. Perfect mixing in the gas phase was proven by measurement of the residence time distribution [29]. This type of reactor has already been used for several gas phase kinetic studies at atmospheric pressure [31], [32] and [33] and at pressures up to 10 bar [34].

The reactor used in this study, made of fused silica (to minimize wall effects), consists of a quartz sphere (volume = 85 cm3) into which diluted reactants enter through four nozzles located at its center, providing turbulent jets for mixing. It is operated at constant temperature and pressure. It is preceded by an annular preheating zone in which gases are progressively heated to the reaction temperature in order to minimize thermal gradients in the gas phase inside the reactor [35]. Gas mixture residence time inside the annular preheater is very short compared to its residence time inside the reactor (a few percent). Both the spherical reactor and the annular preheating zone are heated by resistances rolled up around the walls [36]. The reaction temperature was measured with a type K thermocouple inserted into the intra-annular part of the preheating and the extremity of which was located at the center of the sphere. Uncertainty in the reaction temperature was ±2 K.

The fuel flow rate was controlled by a liquid-mass-flow controller and was mixed with the carrier gas (helium) and then evaporated by passing through a single-pass heat exchanger, the temperature of which was set above the boiling point of the hydrocarbon ($T_{boil,CHX}$ = 354 K). Carrier gas and oxygen flow rates were controlled by gas-mass-flow controllers. The accuracy of the liquid and gas flow rates was around 0.5%. This results in a maximum uncertainty of 2% in the residence time. For both jet-stirred reactor and laminar burning velocity experiments, helium and oxygen were provided by

Messer (99.999% purity for He and 99.995% for O2), and cyclohexane was provided by Riedel-de-Haën (purity ~99.5%).

Experiments were performed under a constant pressure of 1.07 bar (800 Torr), at a residence time of 2 ± 0.04 s, temperatures ranging from 500 to 1100 K, and fuel inlet mole fraction of 0.0067 for equivalence ratios of 0.5, 1, and 2 (equivalence ratio changed by varying O_2 concentration).

2.1.2. Description of the analytical method

The outlet products were analyzed on line using gas chromatography. The online analysis of products that are liquid under standard conditions was made possible by a heated transfer line between the reactor outlet and the chromatograph sampling valves (also heated). During the study, the temperature of the transfer line was set to 413 K. This is an optimum temperature to keep all reaction products in the gas phase and also to prevent their decomposition.

Three gas chromatographs were used for species quantification:

- The first gas chromatograph, equipped with a Carbosphere packed column, a thermal conductivity detector (TCD), and a flame ionization detector (FID), was used for the quantification of O_2, CO, CO_2, methane, ethylene, acetylene, and ethane. Hydrogen could also be quantified using the TCD signal; however, the accuracy in hydrogen mole fraction was not as good as for other species, given that the H_2 peaks were very small due to the use of helium as reference and carrier gas. Therefore, among products that are known as important for hydrocarbon oxidation, only water and hydrogen were not quantified.

- The second gas chromatograph was fitted with a PlotQ capillary column and a FID preceded with a methanizer allowing the quantification of carbon oxides with a better sensitivity than a thermal conductivity detector, as well as the quantification of formaldehyde, and was used for the quantification of C_1–C_5 hydrocarbons and small oxygenated compounds. Figure 1 displays an extract from a chromatogram obtained with the PlotQ column for an experiment performed at a temperature of 850 K, a residence time of 2 s, and an equivalence ratio of 0.5. A very good separation of species is obtained up to C_5 hydrocarbons. The column fails in separating C6 species: the peaks of benzene, cyclohexane, and cyclohexene have very close retention times, with the cyclohexene peak in the tail of the cyclohexane one. The peak of formaldehyde (18–20 min) is very broad, which affects the accuracy of the measurement.

- The third gas chromatograph was fitted with an HP-5 ms capillary column, a FID, and a mass spectrometer (MS). It was used for the quantification of hydrocarbons and oxygenated species with more than five heavy atoms (i.e., carbon and oxygen atoms). The mass spectrometer allowed the identification of heavy reaction products. Figure 2 displays a chromatogram obtained using a HP-5 capillary column for an experiment performed at a temperature of 825 K, a residence time of 2 s, and an equivalence ratio of 0.5. This column provides a better separation of the C6 species: cyclohexene

and cyclohexane peaks are well defined. It also provides a good separation of the numerous $C_6H_{10}O$ isomers that are formed in the low-temperature chemistry of alkanes.

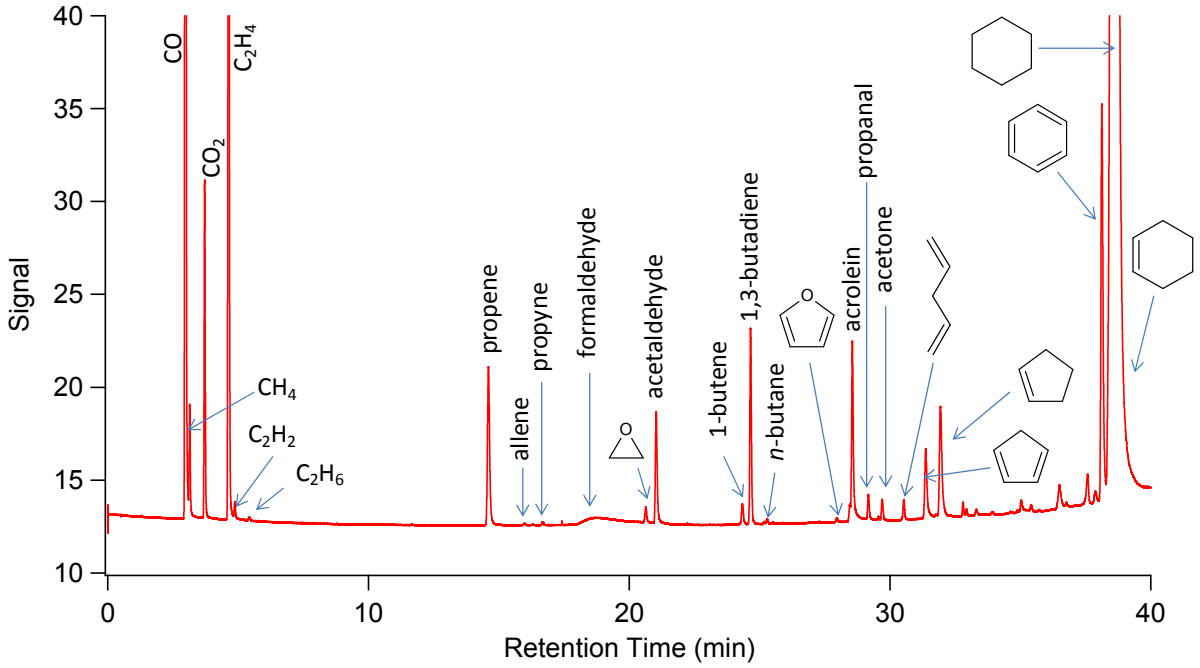

Fig. 1. Chromatogram obtained using a plot Q capillary column for an experiment performed at a temperature of 850 K, a residence time of 2 s, and an equivalence ratio of 0.5.

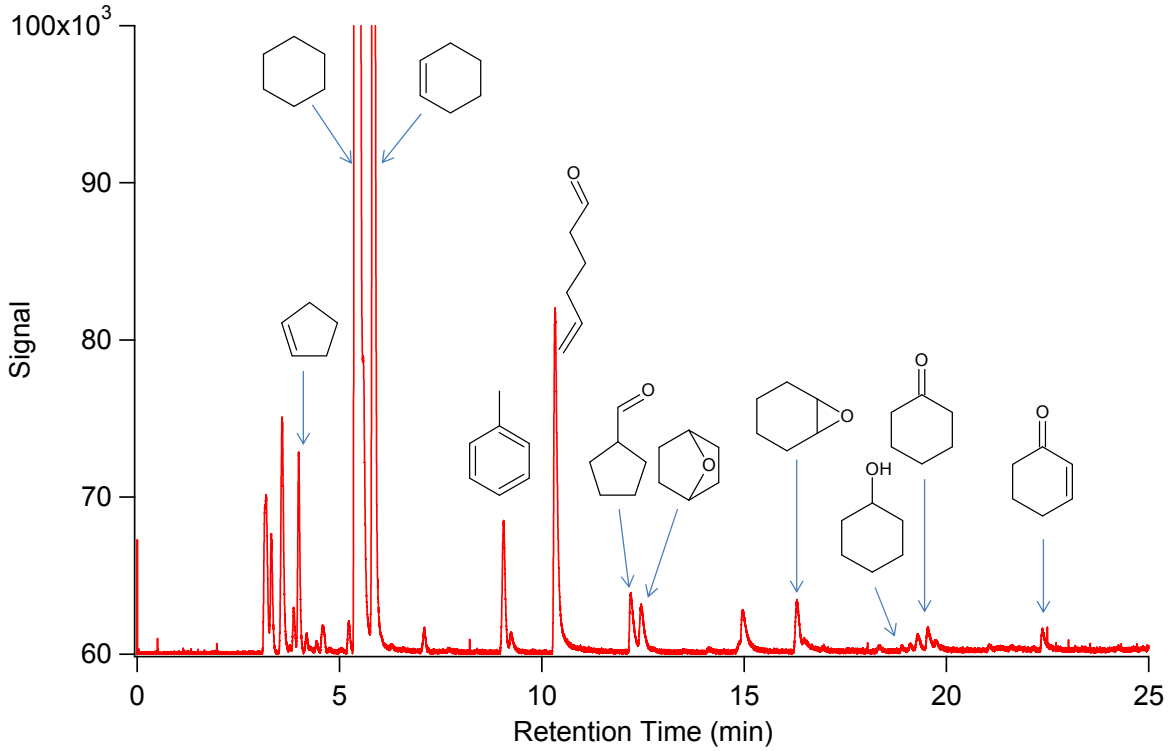

Fig. 2. Chromatogram obtained using an HP-5 capillary column for an experiment performed at a temperature of 825 K, a residence time of 2 s, and an equivalence ratio of 0.5.

The calibration was performed by injecting known amounts of the pure substances when available; otherwise, the method of effective carbon number [37] was used (species having the same number of carbon atoms and the same functional groups were assumed to have the same response in the FID). The identification and the calibration of light species (e.g., oxygen, hydrogen, carbon oxides, formaldehyde, methane, C_2 hydrocarbons, propene, propyne, allene, iso-butene, 1-butene, and 1,3-butadiene) were performed by injecting gaseous samples provided by Messer and Air Liquide. The calibration for the fuel was performed from the analysis of gaseous mixtures of cyclohexane and helium under unreactive conditions. When the quantification was performed using the method of effective carbon number, the reference species with a structure as close as possible to that of the quantified species was used for better accuracy (as an example, the calibration coefficient of cyclohexene was estimated from that of the fuel).

A list of the stable organic species quantified during these experiments is given in Table 2. Carbon balances were done for the lean and rich experiments (formaldehyde not quantified at $\phi = 1$). For the rich mixture, the balance is around 2–3%, with a maximum discrepancy of ±10% (note that the uncertainty in the quantification of the species is about 10%). For the lean one, the balance is between 2–6% with a maximum discrepancy of 20% at 625–650 K. This is due to the fact that as the mixture becomes richer in O_2, more oxygenated species are formed, some of which cannot be identified.

2.2. Laminar flat flame burner experiments

Laminar burning velocity measurements were performed using a recently built flat flame adiabatic burner. This apparatus has already been used for measuring laminar burning velocities of the components and surrogate mixtures of natural gas [38] as well as diethyl ether [39]. The apparatus consists of a burner head mounted on a plenum chamber. The burner head is a thin perforated plate made of brass of diameter 30 mm, which is used to stabilize the flame. Each small hole of the plate has diameter 0.5 mm, and the pitch between the holes is 0.7 mm. Eight type K thermocouples of diameter 0.5 mm are soldered into the plate surface and are positioned at different distances and angles from the center to the periphery of the burner. The plenum chamber is encompassed by a thermostatic oil jacket, the temperature of which is set to the desired initial temperature of the unburned gas mixture. The circumference of the burner plate is heated with thermostatic oil set to 50 K above the temperature of the unburned gas mixture. In practice, if an initial temperature (Ti) of 358 K is desired, the temperature of the plenum chamber is set to 358 K and that of the burner plate to 408 K. Thus, the heat gain of the unburned gas mixture can compensate for the heat loss necessary for stabilizing the flame, knowing that monitoring of the heat loss or gain is performed with the thermocouples. A schematic representation of the burner can be found in [38].

If the unburned gas velocity is lower than the adiabatic flame burning velocity, the sum of the heat loss and heat gain is greater than zero; therefore, the center of the burner plate is hotter than the periphery, and the flame is stabilized under subadiabatic conditions. On the other hand, if the unburned gas velocity is higher than the adiabatic burning velocity, the center of the burner plate is cooler than the periphery, and the flame is stabilized under superadiabatic conditions. Thus, when the temperature profile is flat, it means that no heat is lost or gained by the flame, so that the flame becomes adiabatic with respect to the burner. By changing the flow rate of the gas mixture, it is possible to find an appropriate value of the gas velocity to cancel out the net heat flux, so that the radial temperature distribution in the burner plate is uniform. The flow rate at which the net heat flux is zero corresponds to the adiabatic flame burning velocity [40].

For compounds in the gas state at room temperature, gas flow rates were measured using Bronkhorst High-Tech mass flow controllers (MFC), and for those that are liquid at room temperature, liquid flow rates were measured using a Bronkhorst mini-CORI-FLOW mass flow controller. Synthetic air was used in experiments (O_2:N_2 = 21:79).

As the adiabatic laminar burning velocity is found when the net heat loss is zero, uncertainty is dependent on a few factors. The uncertainty in the laminar burning velocity can be attributed to:

- Uncertainty in the mass flow measurements (around 0.5% for each MFC), which can lead to a global uncertainty of 1.5%.
- Thermocouple readings, which can result in an uncertainty of around 0.2 cm/s.
- Uncertainties due directly to flame distortions, such as edge effects estimated around 0.2 cm/s globally; these effects become more important as the flame is far from stoichiometric conditions (very rich or very lean).

Concerning the calculation of equivalence ratios, note that the main uncertainty is due to the mass flow measurements, which can be estimated as 1%. Finally, there are some qualitative uncertainties, which are difficult to evaluate, such as the possible uncertainty in the fresh gas temperature if the gaseous mixture does not spend enough time in the plenum chamber to reach the desired unburned gas temperature uniformly.

3. Chemical kinetic mechanism

The kinetic mechanism used in this study is based on the previous work of Buda et al. [27]. This mechanism was further revised in 2009 based on the theoretical work of Sirjean et al. [28], who calculated the rate constants for isomerization between cyclohexylperoxy and cyclohexylhydroperoxy radicals as well as the rate constants for decomposition of cyclohexylhydroperoxy radicals into cyclic ethers and OH at the CBS-QB3 level of theory. These reactions are very important in the low-temperature oxidation of cyclohexane and will be discussed along with the experimental results. In view of our experimental results, some reactions have been added to and/or updated from the existing mechanism; the present mechanism is provided as Supplemental material.

The present mechanism was generated using EXGAS [41] and [42], a computer package generating reaction mechanisms describing the gas phase oxidation of linear and branched hydrocarbons. It basically consists of three parts:

- The first part is a C_0–C_2 reaction base that contains the reactions of small species having two carbon atoms or less. The kinetic data used in the C_0–C_2 reactions base were taken from the literature, mainly the values recommended by Baulch et al. [43] and [44] and Tsang and Hampson [45]. Some changes were made to this base, which will be described below.

- The second part is a comprehensive primary mechanism containing the reactions of the reactant and of the radicals deriving from the reactant (with more than two carbon atoms). In the case of cyclohexane, these include unimolecular/bimolecular initiation steps, addition reactions of alkyl and hydroperoxy alkyl (QOOH) radicals to O_2, and isomerizations of R, ROO, and QOOH, as well as beta scission and metathesis reactions [27], [41] and [46]. Note that the improvements for the generation of the reaction of alkenyl radicals proposed by Bounaceur et al. [47] have been taken into account in the generation of the present model; for example, the isomerization of the C_6H_9OO radicals involving a transition state with a double bond in the ring is not considered.

- The third part is a global secondary mechanism that contains the reactions of the molecular products formed in the primary mechanism. EXGAS, for the time being, does not have a secondary reaction base involving the reactions of the cyclic products formed in the primary mechanism. These reactions were therefore introduced manually, following rules similar to those used for linear compounds [48].

Thermochemical data for molecules or radicals are automatically calculated and stored as 14 polynomial coefficients; these are calculated using the software THERGAS [49] based on the group

and bond additivity methods proposed by Benson [50]. Thermodynamic properties of some cyclohexane derived species were calculated by Sirjean et al. and are listed in [51]. The transport properties of the species were evaluated by using an in-house code for species for which no data were available (mainly species not included in the C_0–C_2 reaction base). Correlations proposed by Wang and Frenklach [52] were used for the estimation of the Lennard–Jones collision diameter and of the Lennard–Jones potential well depth from the molecular weight. A value of zero was assigned to the dipole moment and to the polarizability, as there are no accurate correlations available for these parameters and as these parameters are expected to be close to zero. The rotational relaxation collision number at 298 K was set to a value of 1, as for many species in the C_0–C_2 reaction base. We will describe hereafter the modifications introduced into the automatically generated mechanism, with the aim of better consideration of the specificities of cyclohexane oxidation chemistry.

3.1. C_0–C_2 chemistry

As stated above, the rate constant values for the C_0–C_2 reaction base in EXGAS are based on well-established values from the literature. Recently, the rate constants of the reactions $CO+HO_2 \leftrightarrows CO_2+OH$ and $CH_2O+OH \leftrightarrows HCO+H_2O$ were modified. The rate constant for the former reaction is taken as $1.57 \times 10^5 T^{2.18}$ exp (−17,900/RT) $cm^3\ mol^{-1}\ s^{-1}$, proposed by You and co-workers [53] based on an ab initio study, and for the latter reaction as $7.87 \times 10^7 T^{1.63}$ exp (1063/RT) $cm^3\ mol^{-1}\ s^{-1}$, proposed by Vasudevan et al. [54] based on experimental results at high temperatures, which are fitted to the low-temperature measurements from the literature in order to get an expression in a wider interval. These are the updated values used in the present mechanism. Another modified base mechanism reaction is the pressure-dependent $H_2O_2(+M) \leftrightarrows OH+OH(+M)$ for both dissociation of H_2O_2 and reverse recombination of the OH radicals; we have adopted the recent evaluations of Troe [55].

3.2. Hydrogen abstraction reactions

Hydrogen atoms in cyclohexane are considered as 12 equivalent secondary hydrogen atoms in a noncyclic alkane. No further modification has been made in the present study. In cyclohexane oxidation, in our temperature interval of interest, hydrogen abstraction reactions by mostly OH and H and to some extent (intermediate temperatures) by HO_2 radicals are of importance. Since the propagation step $cyC_6H_{12}+OH \leftrightarrows cyC_6H_{11}+H_2O$ is very sensitive under all conditions, we compared our estimation of $1.6 \times 10^7 T^2$ exp (765/RT) $cm^3\ mol^{-1}\ s^{-1}$ with the available literature data (Fig. 3).

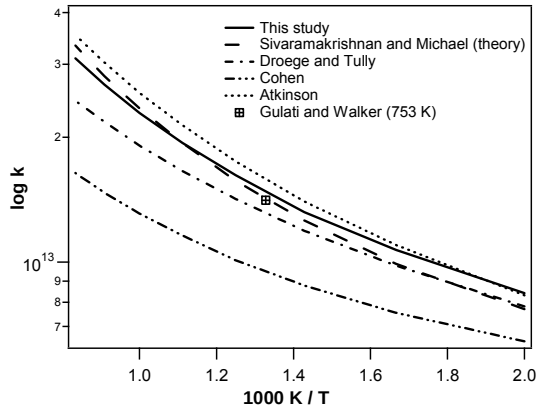

Fig. 3. Rate constant expressions for the reaction $cyC_6H_{12}+OH \leftrightarrows cyC_6H_{11}+H_2O$ [6], [56], [67] and [68].

The only experimental determinations in our temperature range (T > 500 K) are reported by Gulati and Walker [6] and Sivaramakrishnan and co-workers [56]. The former study reports a measurement at 753 K, while the latter reports measurements between 801 and 1347 K, and also includes the calculation of this rate constant on a G3//B3LYP level of theory. The rate constant adopted in this study is in very good agreement with both studies. On the other hand, our rate constant is 1.75 times higher (at 1000 K) than the one calculated by Cohen [57] via transition state theory. Further discussion on metathesis and on other sets of reactions used in the EXGAS database is detailed in Heyberger et al. [58] and Warth et al. [41].

3.3. Dissociation of the cyclohexylhydroperoxy radicals

The cyclohexyl radical (cy-C_6H_{11}) formed as a result of metathesis reactions either adds to molecular oxygen to form the cyclohexylperoxy radical (cy-$C_6H_{11}OO$) at low temperatures, goes through beta scission via ring opening, or yields cyclohexene (cy-C_6H_{10}) via oxidation and/or dehydrogenation at higher temperatures. The cy-$C_6H_{11}OO$ radical formed at low temperatures isomerizes into cyclohexylhydroperoxy radicals (cy-$C_6H_{11}OOH$) by internal hydrogen transfer through 4-, 5-, 6-, or 7-membered transition states (see scheme below), which then dissociate into cyclic ethers and OH, as globally represented in the scheme in Fig. 4.

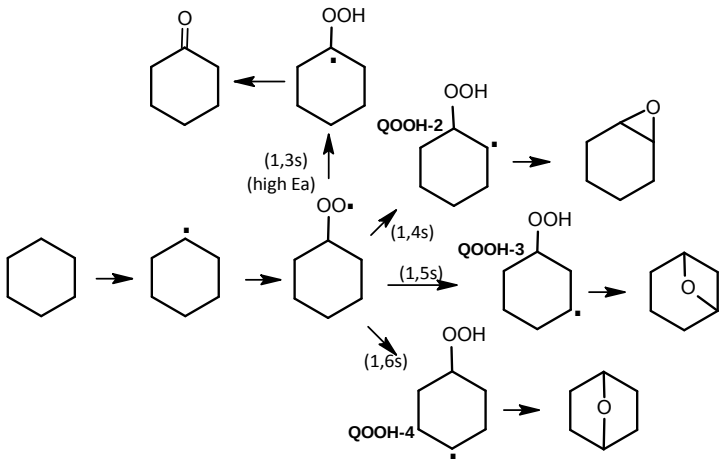

Fig. 4. Oxidation chemistry of the cyclohexyl radical (cy-C_6H_{11}). Formation routes of $C_6H_{10}O$ cyclic ethers and cyclohexanone.

Rate constants corresponding to these isomerization and cyclic ether formation reactions are calculated and discussed by Sirjean et al. [28] and are used in this study. However, the A-factors of the QOOH dissociation reactions are reduced by a factor of 10, while the isomerization rate constants are used without a change. In fact, there is a disagreement in the literature about the values of the QOOH decomposition rate constants. Cavallotti et al. [59] calculated kinetic parameters of $RO_2 \leftrightarrows$QOOH isomerization and QOOH decomposition reactions (into cyclic ethers) using a modified G2MP2 approach, while Sirjean et al. [28] calculated on a CBS-QB3 level. On the other hand, the Silke et al. [25] mechanism uses Milano rate constants for QOOH decomposition with activation energies reduced by a few kcal in order to ensure better agreement with experimental data. These rate constants are plotted in Fig. 5; we can observe a large discrepancy, about 1–3 orders of magnitude, in the range of this plot. The LLNL values remain between the other two; however, the discrepancy is still significant. Further investigations are probably needed to provide an answer to this disagreement, which is beyond the scope of this study. The dissociation rate constants used in this study remain between the computed values [28] and [59] and are faster than the ones used in the Livermore mechanism [25], except for the dissociation to 1,4-epoxycyclohexane, where they are in agreement. It is to be noted that similar uncertainties are present for cyclic ether formation from hydroperoxy alkyl radicals in alkane oxidation as well. Computed rate constants from Villano et al. [60], Miyoshi [61], Cord et al. [62], and Wijaya and co-workers [63] are plotted for oxirane, oxetane, and oxolane formation from a secondary QOOH radical and can be found in the Supplementary material. The discrepancies for this specific case amount to 1–3 orders of magnitude.

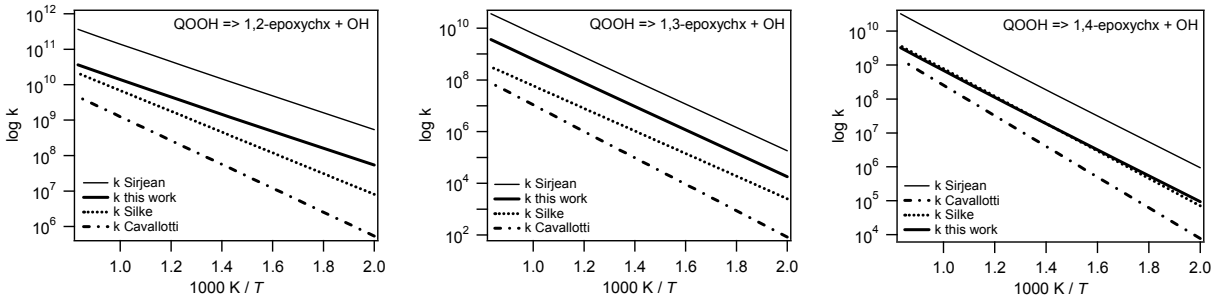

Fig. 5. Rate constants for QOOH decomposition into 1,2-, 1,3-, and 1,4-epoxycyclohexane. Solid lines: Sirjean et al. [28]; dash-dotted lines: Cavallotti et al. [59]; dashed lines: Silke et al. [25]; solid bold lines: rate constants used in this work.

The 1,3-epoxycyclohexane, being unstable, rapidly yields 5-hexenal and was not experimentally identified in this study. The Walker group [6] and [7] observed no 1,3-epoxycyclohexane formation in their experiment, and neither did Yang and Boehman [23] in their engine study. Both groups observed 1,2-epoxycyclohexane, 5-hexenal, and 1,4-epoxycyclohexane, among other products. However, this cyclic ether was identified by Lemaire et al. [11] in their RCM. 5-Hexenal can lose its aldehydic hydrogen through radical attack; in this study, we have also considered hydrogen abstraction at the allylic site, which can become competitive as well. The corresponding rate constants were attributed by assuming two equivalent secondary allylic hydrogen atoms.

Cyclohexene is an important product of the primary oxidation mechanism of cyclohexane in our experiments and also observed experimentally in the literature in different types of apparatus [11], [14], [15] and [23]. At higher temperatures (T > 800 K), cyclohexene is formed via oxidation of the cyclohexyl radical (cy-C_6H_{11}+O_2⇆cy-C_6H_{10}+HO_2) and H-elimination (cy-C_6H_11⇆cy-C_6H_{10}+H) reactions. At lower/intermediate temperatures, concerted HO2 elimination from cyclohexylperoxy radicals (cy-C_6H_{11}OO⇆cy-C_6H_{10}+HO_2) can become competitive with cyclohexyl oxidation. This pathway was not previously considered in the mechanism of Buda et al. [27]. The activation energy for this reaction is taken as 32.1 kcal/mol, as recommended by Simmie [64], which is 1 kcal higher that calculated by Knepp and co-workers [65]. Cyclopentene and 1,3-cyclopentadiene are experimentally observed in this study as secondary reaction products. Given the lack of experimental determinations and/or calculations regarding the corresponding rate constants, cyclopentene ring opening to 1,4-pentadiene and concerted H2 elimination to yield 1,3-cyclopentadiene are considered analogous to those for cyclohexane and rate constants were attributed accordingly. Another secondary reaction product observed in these experiments in both low- and high temperature regions was 2-cyclohexen-1-one with a maximum value of 60 ppm; we have considered its formation through the scheme in Fig. 6.

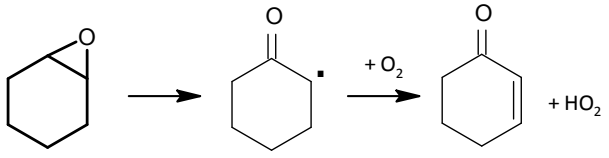

Fig. 6. Reaction added in the model to account for the formation of 2-cyclohexen-1-one.

4. Results and discussion

The model developed in this study was compared with jet-stirred reactor data and laminar flame velocities obtained in the present work.

4.1. Jet-stirred reactor results

The experiments were conducted at equivalence ratios of 0.25, 1.0, and 2.0 at a constant fuel concentration of 0.667% and varying O_2 concentrations. Figure 7 represents fuel, O_2, CO, and CO_2 evolution as a function of temperature. Fuel decomposition shows that cyclohexane displays high low-temperature reactivity with well-marked NTC behavior for lean and stoichiometric mixtures, this behavior is almost insignificant for the rich mixture. For both ϕ = 0.5 and ϕ = 1.0 mixtures, low-temperature reactivity begins at around 600 K and is highest in the vicinity of 625 K; the lean mixture shows highest reactivity with a larger NTC extent. These results are qualitatively consistent with the recent ethylcyclohexane experiments performed by Husson et al. [66] in the same reactor. The model, on the other hand, captures the reactivity of the stoichiometric mixture very well, but shows lower reactivity for the lean mixture and higher reactivity for the rich mixture at low temperature than in the data.

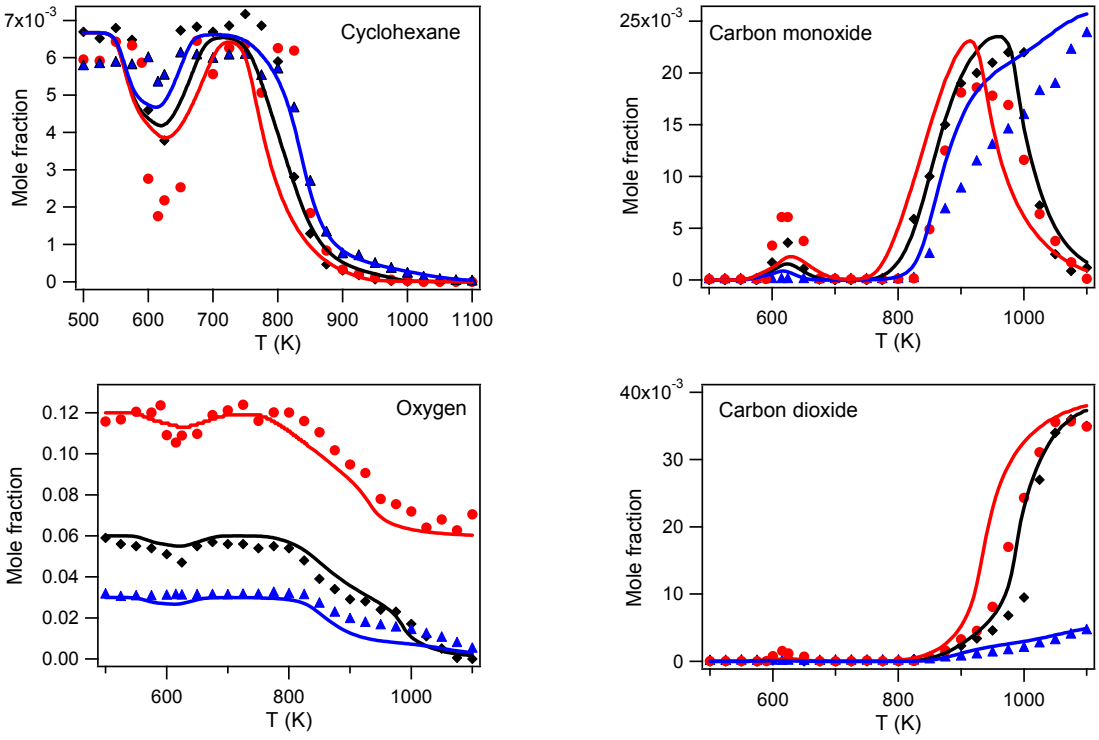

Fig. 7. Mole fractions of cyclohexane, O_2, CO, and CO_2: (▲) ϕ = 2.0; (♦) ϕ = 1.0; (●) ϕ = 0.5. Symbols represent experiments and lines represent model simulations.

The effect of oxygen concentration can be observed for carbon monoxide and carbon dioxide profiles where the lean and stoichiometric mixtures have higher CO to CO_2 conversion above 800 K. The profiles of saturated and nonsaturated linear C_1–C_4 compounds are presented in Fig. 8. In the low-temperature reactivity zone, only some formation of ethylene (170 ppm max) and butenes (20 ppm max) is observed. These species are formed in considerable quantities, especially as the mixture becomes leaner in oxygen. Methane and ethylene are the most important ones, with peak values of 1000 and 3000 ppm for the stoichiometric mixture, respectively. Model results globally agree with the general tendency; however, propene concentration is underpredicted under fuel-rich conditions because its production is mostly due to hydroperoxy radical decomposition in the lumped secondary mechanism, which is more important for the fuel-lean conditions.

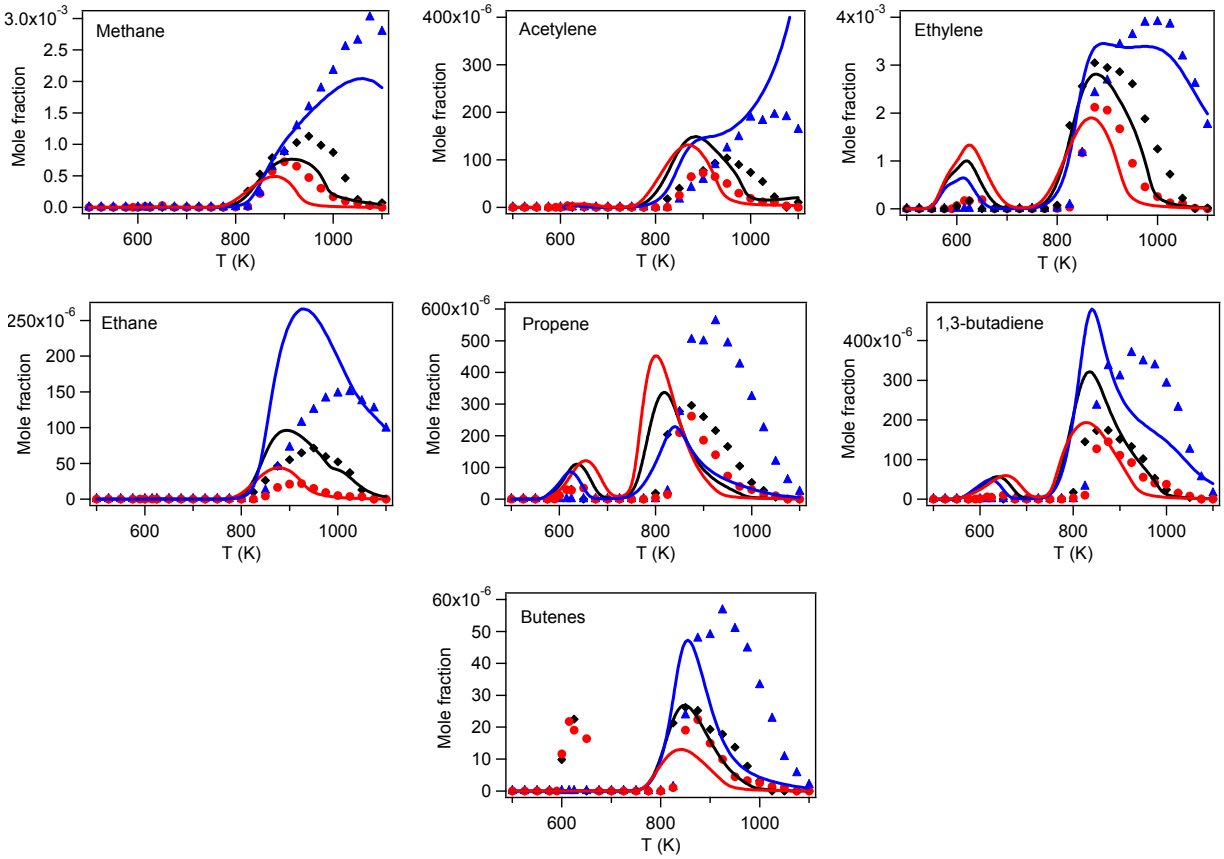

Fig. 8. Mole fractions of C_1–C_4 linear nonoxygenated compounds (CH_4, C_2H_2, C_2H_4, C_2H_6, C_3H_6, 1,3-C_4H_6, sum of 1- and iso-C_4H_8): (▲) ϕ = 2.0; (♦) ϕ = 1.0; (●) ϕ = 0.5. Symbols represent experiments and lines represent model simulations.

Figure 9 represents the mole fractions of the C_1–C_3 oxygenated compounds detected in this experiment. The most important among these is formaldehyde, which peaks between 1200 and 2000 ppm over the whole temperature range, followed by acetaldehyde and acrolein. Part of low-temperature formaldehyde formation results from ketohydroperoxide decomposition that occurs in this temperature range, explaining the high amounts related to it. All of these oxygenated species were detected under both low- and high-temperature conditions, with a low-temperature reactivity

almost as high as the high-temperature reactivity, except for acrolein, which is more abundant at higher temperatures. Given the fact that negligible low-temperature experimental reactivity was observed under rich conditions, no species formation is observed; however, model predictions show some fuel conversion and hence species formation. We also observe that both experimental and model-predicted high-temperature formation of ethylene oxide, acetaldehyde, acrolein, and propanal show little sensitivity to equivalence ratio (O_2 concentration) for lean and stoichiometric mixtures; however, this difference in selectivity is more significant for nonoxygenated compounds, as shown in Fig. 8. The important C_1–C_3 oxygenated compound profiles are satisfactorily reproduced by the kinetic model. Acetaldehyde and acrolein formation in the whole temperature range is predicted very well; both are detected up to 500 ppm. Formaldehyde and ethylene oxide formation is well represented at T > 800 K, while the model fails to reproduce ethylene oxide formation at low temperatures. The formation of ethylene oxide is due to ethylene reactions with radicals such as HO_2 and CH_3O_2; at low temperatures, less ethylene is formed and is mostly consumed via reactions with OH and addition with H. Only 5–6% of the ethylene forms ethylene oxide in the vicinity of 650 K. On the other hand, propanal, which is formed in very small quantities, is not reproduced by the model in either temperature range, probably because of missing formation pathways.

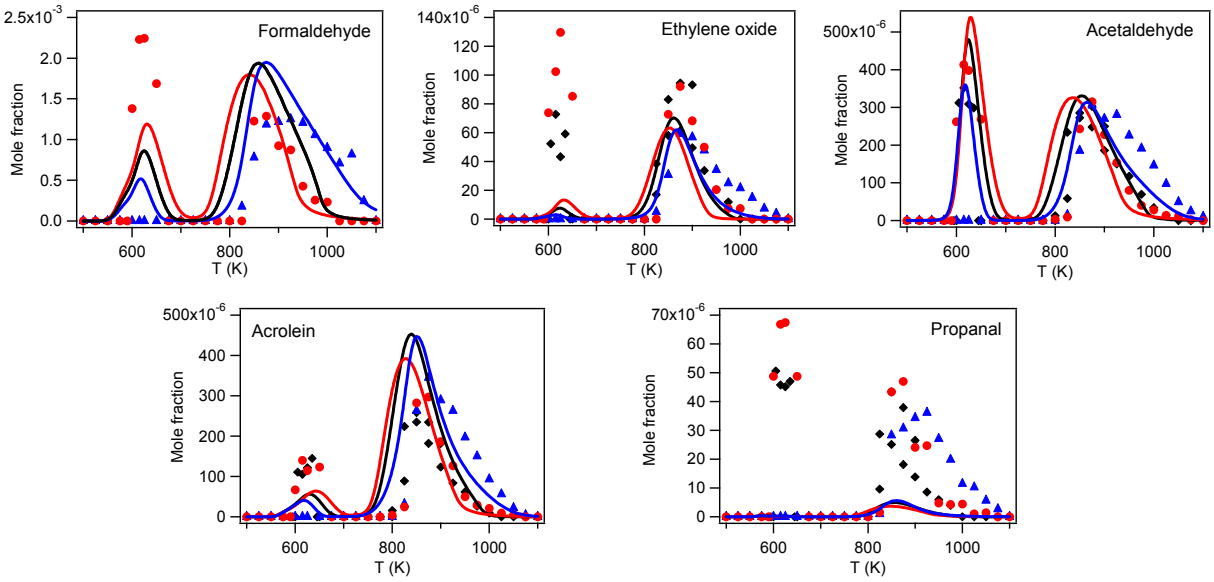

Fig. 9. Mole fractions of C_1–C_3 oxygenates (CH_2O, C_2H_4O, CH_3CHO, C_2H_3CHO, C_2H_5CHO): (▲) ϕ = 2.0; (♦) ϕ = 1.0; (●) ϕ = 0.5. Formaldehyde not quantified at ϕ = 1.0. Symbols represent experiments and lines represent model simulations.

Figure 10 represents the evolution of the mole fraction of cyclic species and 5-hexenal, which is believed to be formed through rapid decomposition of the unstable 1,3-epoxycyclohexane. Among these reaction products, cyclohexene is the most abundant, being produced under both low- and high-temperature conditions in comparable amounts, with peaks of 455 and 645 ppm (at ϕ = 1), respectively. The kinetic model underpredicts cyclohexene formation below 650 K by a factor of 2 for lean and stoichiometric mixtures; at higher temperatures, while the model is in reasonable agreement for the lean mixture, there is an underprediction for the rich one by about a factor of 3.

Other important reaction products are benzene, cyclopentene, and cyclopentadiene, formation of which is favored at higher temperatures; the former two are detected with mole fractions above 200 ppm. The kinetic model is in good agreement with those products for stoichiometric and rich mixtures, while cyclopentene and cyclopentadiene are overpredicted for the lean mixture by about a factor of 2. Another high-temperature product is phenol, which is formed via benzene and is experimentally quantified as less than 70 ppm. 5-Hexenal (not calibrated by an external standard) is experimentally detected in quantities less than 200 ppm; however, the model overestimates its formation at all temperatures, by a factor of 2 at the high-temperature peak and by a factor of ~4 at the low-temperature peak for the stoichiometric mixture. Cyclohexanone, cyclohexanol, 2-cyclohexenone, phenol, and 1,4-epoxycyclohexane are all detected below 100 ppm.

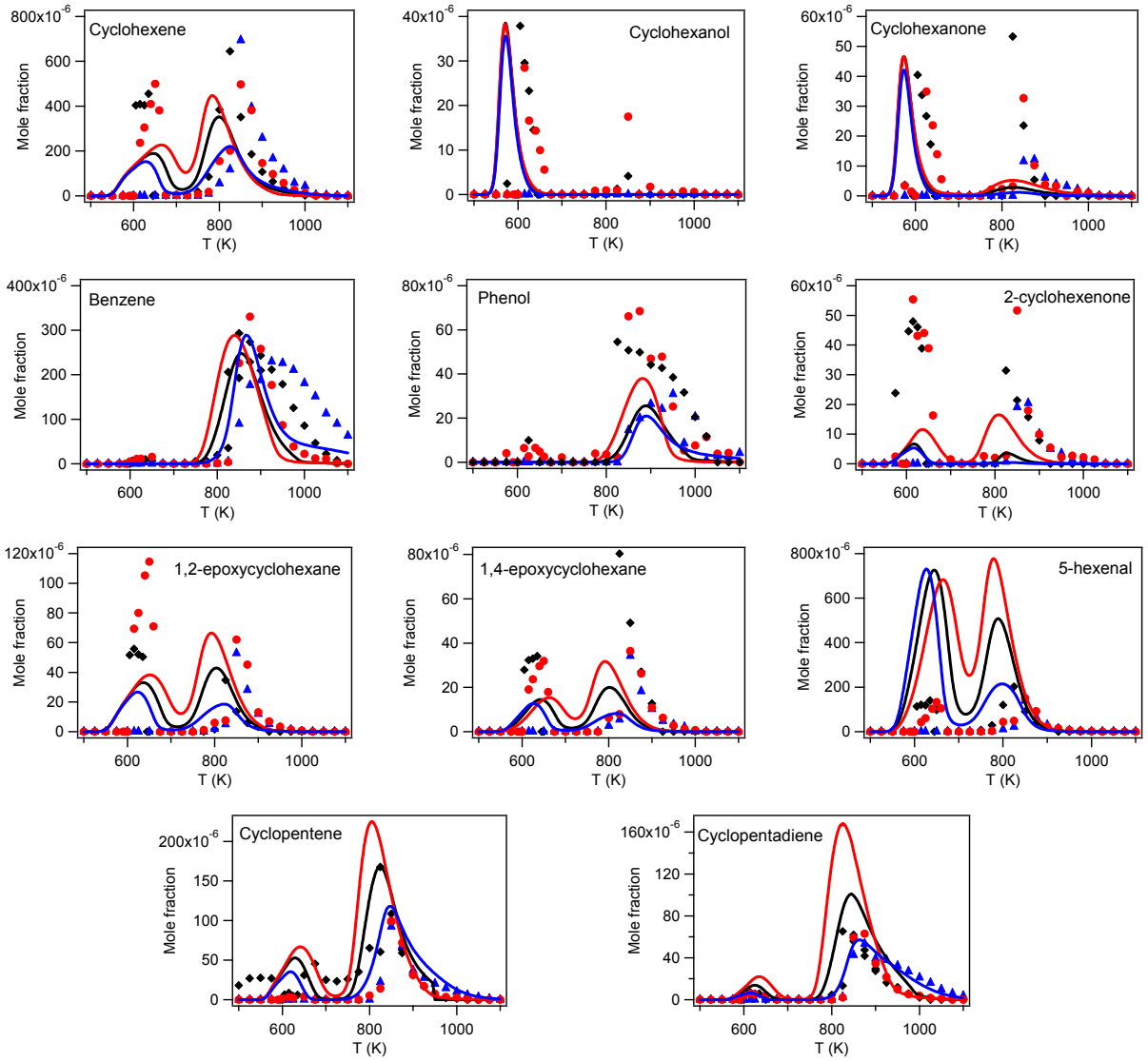

Fig. 10. Mole fractions of cyclic products and 5-hexenal: (▲) ϕ = 2.0; (♦) ϕ = 1.0; (●) ϕ = 0.5. Symbols represent experiments and lines represent model simulations.

Also note that higher temperature (T > 700 K) jet-stirred reactor experiments for cyclohexane by El-Bakali et al. [15] are also simulated by the present mechanism, and the results are presented in the Supplementary material.

4.2. Laminar burning velocity results

Cyclohexane laminar burning velocities are measured at 1 atm and initial temperatures of 298, 358, and 398 K, as explained in the Experimental section of this paper. These results are presented along with the available literature data in Fig. 11a. A peak burning velocity of 40.0 cm/s is observed at an unburned gas temperature of 298 K, and as expected, this value increases as the initial temperature increases; it corresponds to 52.9 cm/s at 358 K and 63.1 cm/s at 398 K, an equivalence ratio of 1.1 for all cases.

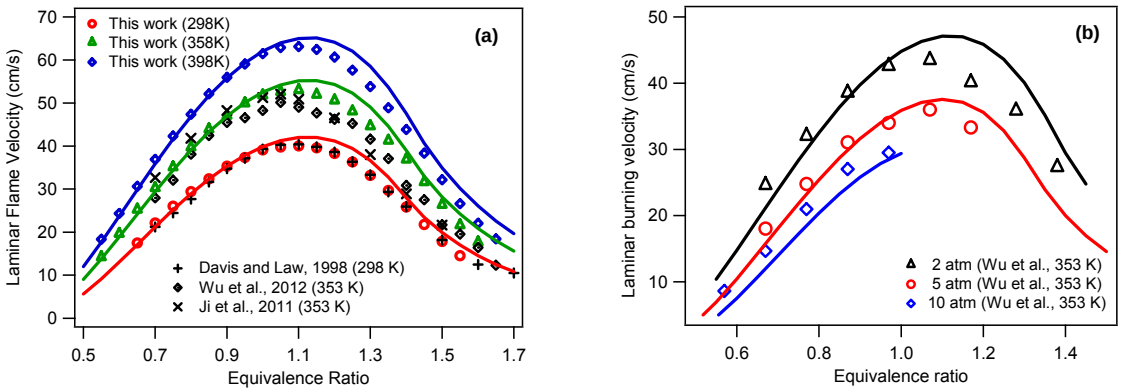

Fig. 11. Cyclohexane laminar burning velocity at (a) P = 1 atm [16], [17] and [18], (b) P = 2, 5, and 10 atm [16]. Closed symbols: this work; open symbols: literature data; lines: simulations.

We can compare our measurements with the literature data for Ti = 298 K and 353 K; however, there are no available data at higher temperatures to make a comparison possible. Davis and Law [17] measured the burning velocity of cyclohexane in a counterflow flame at an unburned gas temperature of 298 K, and these measurements are in excellent agreement with the present ones. More recently, Ji et al. [18] measured the burning velocity of cyclohexane (□) in a counterflow configuration at an unburned gas temperature of 353 K, and Wu et al. [16] measured the burning velocity of cyclohexane (○) in an expanding spherical flame at 353 K and at pressures up to 20 atm. Even though in our measurements, the unburned gas temperature was 358 K, a comparison is still possible (keeping in mind that a higher initial temperature would result in a higher flame speed). Our measured peak point agrees well with the one measured by Ji et al. [18]; however, Wu et al. [16] measured a peak value corresponding roughly to ϕ = 1.0. Between the present data and these two studies, the agreement deteriorates under rich conditions: a gap of 5 cm/s is observed in the vicinity of ϕ = 1.2. The kinetic model is generally in good agreement with the data, especially in the lean and rich zones; there is an overprediction of about 3 cm/s in the peak burning velocity at all unburned gas

temperatures. Figure 11b represents measurements by Wu and co-workers [16] at higher pressures (2, 5, and 10 atm), and our simulation results show good agreement, especially for the 5- and 10-atm cases. As far as the 2-atm data are concerned, a 2–4 cm/s discrepancy is observed under the rich conditions, similarly to 1 atm simulations.

5. Reaction path analysis

Cyclohexane exhibits a low-temperature chemistry very similar to that of normal alkanes, which is generically represented in the scheme in Fig. 12.

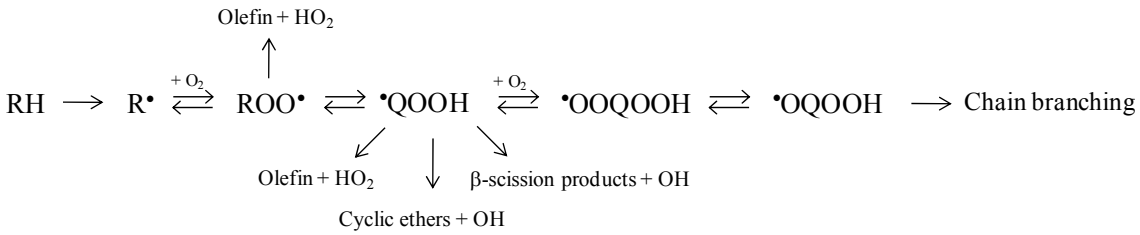

Fig. 12. Low-temperature oxidation chemistry scheme for normal alkanes.

Globally speaking, fuel conversion mostly occurs by attack of OH radicals abstracting a hydrogen atom; in the intermediate temperature zone, metathesis reactions by HO_2 and H become significant as well. These reactions produce cyclohexyl radicals (cy-C_6H_{11}), most of which (>90%) adds to molecular oxygen to form cyclohexylperoxy radicals (cy-$C_6H_{11}OO$) at low temperatures, on the other hand, ring opening to form hexenyl radicals is favored at higher temperatures. Isomerization of the cy-$C_6H_{11}OO$ yields cyclohexylhydroperoxy radicals (cy-$C_6H_{11}OOH$), among which the product of the 1,5 hydrogen shift reaction (meta-cyclohexylhydroperoxy) is highly favored; this QOOH radical produces 5-hexenal through ring opening (1,3-epoxycyclohexane being unstable). To understand the reaction paths and their relative importance for our system, reaction path analyses were performed at 850 K for all mixtures, and at 600 K for the stoichiometric and lean mixtures. Rich mixture was omitted for the 600 K analysis, given that no experimental reactivity was observed. Let us recall that fuel mole fraction was kept constant at 6.67×10^{-3} and O_2 concentration was varied in order to change the equivalence ratio in our experiments. Cyclohexane conversion for the stoichiometric mixture corresponds to 61.6% and 34.3% at 850 and 600 K, respectively.

5.1. Reaction paths at 850 K

Figure 13 represents the reaction paths for all mixtures at 850 K. At this temperature, cyclohexane is consumed by H-abstraction reactions, mostly by OH radicals (75% and 87% of fuel consumption at ϕ

= 2.0 and 0.5, respectively) followed by H and HO_2 to give cy-C_6H_{11} radicals. There are three possible ways to consume the cy-C_6H_{11} radicals; among these, ring opening via reaction 1 is highly favored, especially for the rich and stoichiometric mixtures.

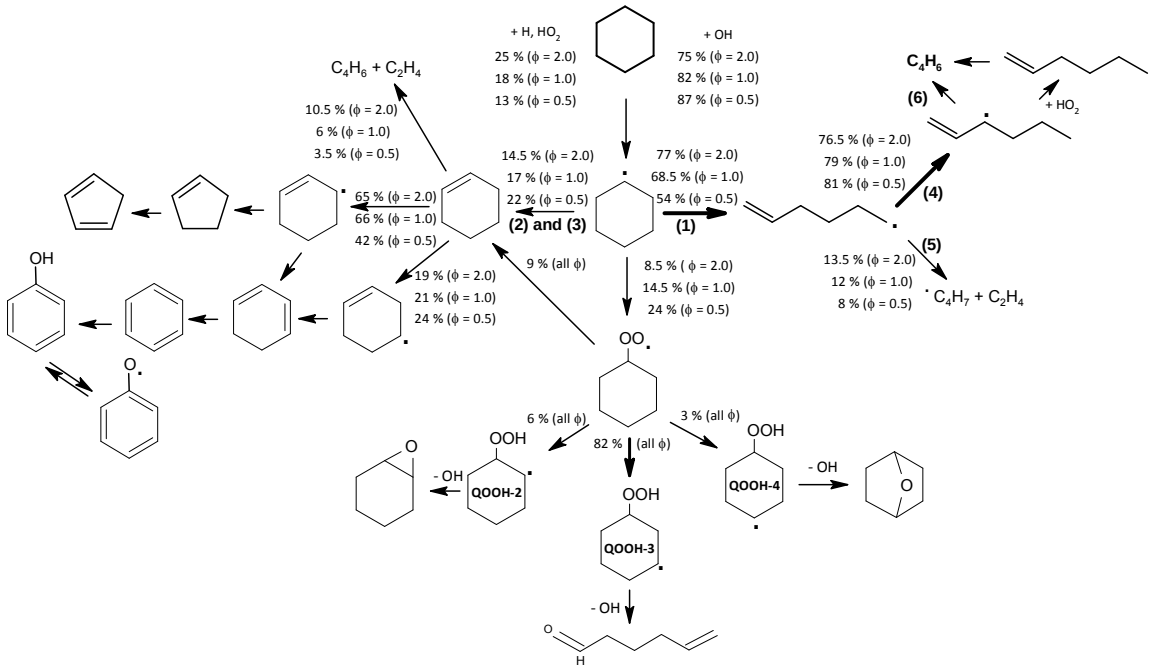

Fig. 13. Reaction paths for all mixtures (ϕ = 0.5, 1.0, and 2.0) at 850 K.

As far as the rich mixture is concerned, 77% of the cy-C_6H_{11} radicals are consumed this way, and only 8.5% consumption is observed to be through O_2 addition, because of the lower abundance of O_2 for this mixture (3% as opposed to 12% for the ϕ = 0.5 mixture). The rest goes through either oxidation or H-elimination to form cyclohexene (reactions 2 and 3). On the other hand, the lean mixture has more available molecular oxygen, and addition to O_2 and oxidation to cyclohexene become more important and consume 46% of the cy-C_6H_{11} radicals altogether. Cyclohexene is consumed via metathesis reactions by OH and H to yield alkylic-, allylic-, and vinylic-type cyclohexenyl radicals, depending on the abstraction site; among these, the vinylic radical is negligible, given the very high bond dissociation energy of this type of C–H bond. Among the final products observed in the cyclohexene pathway, cyclopentene, cyclopentadiene, benzene, and phenol were experimentally detected, while 1,4- or 1,3-cyclohexadiene were not. The model calculation agrees with this observation predicting only a few ppm of this intermediate molecule at 850 K, flux analysis shows that it is in fact rapidly decomposed to its radical, which mostly reacts through hydrogen elimination, which is responsible for the formation of benzene.

Among the possible isomerization pathways for the 1-hexenyl radical as represented in Fig. 13, reaction 4 is favored; more than 76% of the radical formed is consumed this way. Beta scission (reaction 5) also occurs to some extent and is responsible for 10% of ethylene formation for the stoichiometric mixture. The hexenyl isomer formed via reaction 4 mostly goes through beta scission (reaction 6) to yield 1,3-butadiene and ethyl radicals (~50% of the 1,3-butadiene formation is due to

this reaction); it can otherwise add to molecular oxygen or form 1-hexene and 1,2-hexadiene (minor pathway), none of which were detected experimentally. Note that addition reactions of the alkenyl radicals to O_2 are negligible in the whole temperature interval, given that at low temperatures, addition of cy-C_6H_{11} radicals to O_2 is favored over ring opening, and at high temperatures, the alkenyl radicals formed go through isomerization and dissociate via beta scission. At 850 K, some cy-C_6H_{11} adds to molecular oxygen, similarly to the low-temperature scheme that will be discussed in the coming section. For the lean mixture this amounts to 24% of consumption given the abundance of oxygen.

5.2. Reaction paths at 600 K

Figure 14 represents reaction paths for lean and stoichiometric mixtures at 600 K. In agreement with the generic alkane low-temperature oxidation scheme, $R+O_2 \leftrightarrows RO_2$ proceeds in favor of cy-$C_6H_{11}O_2$ formation; only 6% of the cy-C_6H_{11} radicals go through oxidation to form the conjugated olefin. Isomerization products of the cy-$C_6H_{11}O_2$ radicals are three-fold; isomerization to the 1-hydroperoxycyclohexyl radical is neglected, given the high activation energy associated with this reaction. Among the cy-$C_6H_{10}OOH$ radicals, the product of the 1,5-hydrogen shift reaction (3-hydroperoxycyclohexyl radical) is highly favored. It is to be noted that at this temperature, the rate constant associated with the 1,5 shift isomerization reaction (leading to the meta-radical) is faster by about two orders of magnitude than that of 1,4 and 1,6 shift reactions [28] and [59]. Only a very small part (<5%) of the cy-$C_6H_{10}OO$ forms cyclohexanone and cyclohexanol, mostly via $RO_2 + RO_2$ and partly via $RO_2 + CH_3O_2$ disproportionation reactions.

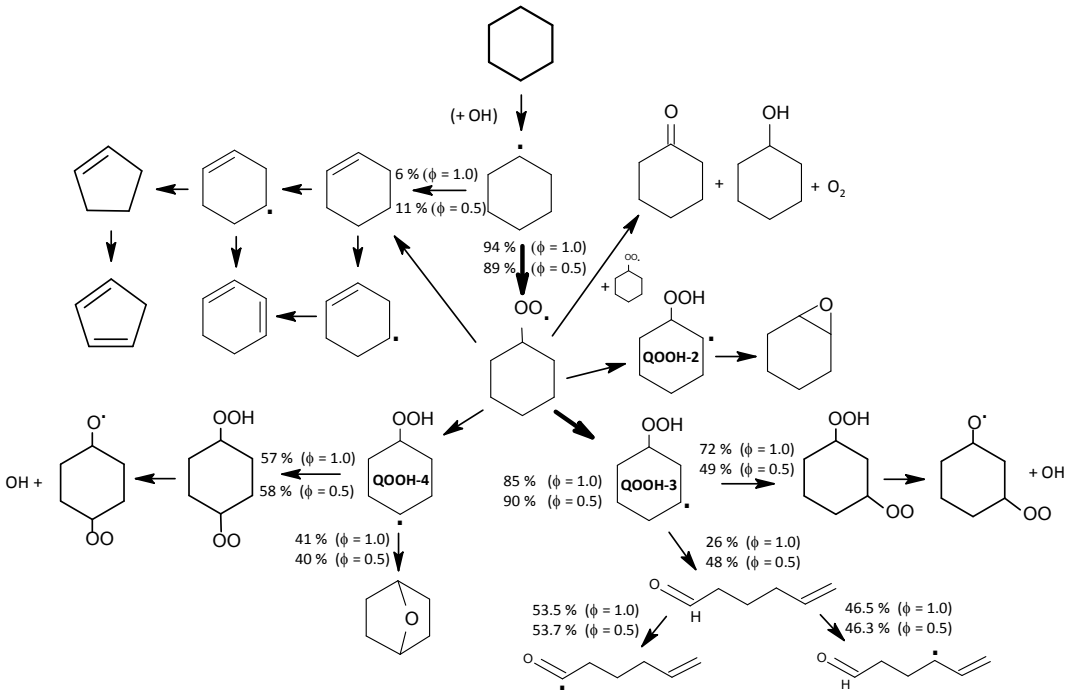

Fig. 14. Reaction paths for stoichiometric and lean mixtures at 600 K.

The cy-$C_6H_{10}OOH$ radicals then decompose into cyclic ether and OH or add to molecular oxygen to form the OOQOOH radicals, which form ketohydroperoxides and OH. In both our schemes, 5-hexenal is presented as the decomposition product of the meta-hydroperoxycyclohexyl radical, given that the 1,3-epoxide is unstable and rapidly decomposes. Metathesis of 5-hexenal yields aldehydic and allylic radicals in almost equal quantities; these radicals further lead to the production of formaldehyde, acetaldehyde, propene, and 1,3-butadiene, which are important low-temperature products.

6. Rapid compression machine and shock tube simulations

Cyclohexane oxidation was studied in a RCM by Lemaire et al. [11] and more recently by Vranckx et al. [12] in the NTC region; the ignition delay data and our simulation results are presented in Fig. 15. In the same figure are also represented the shock tube ignition delay time data from Daley et al. [9], given that their experimental conditions were complementary to both RCM conditions on a temperature scale; they used cyclohexane mixtures in synthetic air and the reflected shock pressure was between 13 and 15 bar. All RCM simulations were performed taking into account the Aachen initial conditions at constant volume and without considering any heat loss. The simulations of the data [15] that could not be presented in Fig. 15 are provided as Supplementary material.

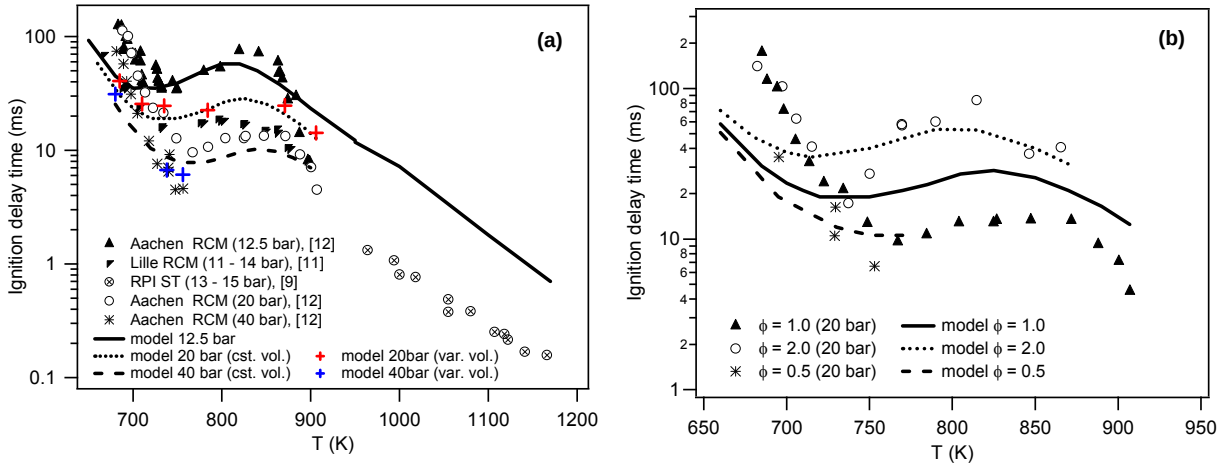

Fig. 15. Cyclohexane ignition delay times in two rapid compression machines [11] and [12] and a shock tube [9]; (a) Aachen/Lille RCM and ST ignition delay times at various pressures and ϕ = 1.0; (b) Aachen RCM, p = 20 bar at various equivalence ratios and constant x_{fuel} = 0.0226.

Figure 15a represents RCM [11] and [12] and ST [9] ignition delay times for ϕ = 1.0 and at compressed gas pressures varying from 11 to 40 bar. Both the Lille and Aachen RCM experiments use the same stoichiometric ratio (ϕ = 1, O_2/inert = 0.27); they can therefore be considered as performed under identical conditions. Both experiments show a strong negative temperature dependence of cyclohexane, even though the Lille data appear to be significantly slower than the Aachen data. These quantitative differences can be attributed to the differences between the two setups, such as

heat loss and/or compression times; longer compression times can allow chemistry to occur during compression, resulting in shorter ignition delay times. Moreover, it is to be noted that our simulations (lines) were performed assuming no heat loss and could therefore be faster, especially in longer ignition delay time zones (up to 700 K and between 780 and 830 K). Further simulations were performed at selected experimental points at compressed pressures of 20 and 40 bar by introducing a volume history. This procedure resulted in longer ignition times at low temperatures, up to 33% of the constant volume simulations (colored points in Fig. 12a). At higher temperatures, no significant difference was observed, except for the 40-bar case where the ignition delay time is 35% faster. On the other hand, the RPI shock tube data are highly overpredicted, even though the model curve is consistent with the RCM predictions.

In Fig. 15b, ignition delay times measured (Aachen RCM) at a compressed gas pressure of 20 bar and at a constant fuel fraction of 0.0226 are represented, along with model simulations. Both experimental measurements and simulations show that ignition delay times converge at the lowest investigated temperatures; the model prediction is faster here, as explained above. The experiment shows much more pronounced NTC behavior for the rich mixture; however the model predictions are quite similar in terms of reactivity range in this region. At T > 750 K, model predictions agree with the data for the rich mixture; however, they are slower by about a factor of 2 for the stoichiometric mixture. The simulations for the lean mixture above 750 K were performed for comparison purposes.

Figure 16 represents shock tube data from the Stanford group [8] in 16a and the Nancy group [10] in 16b. Both experiments were performed under dilute conditions, using argon as bath gas. The reflected shock pressure (P_5) was 1.5 and 3 atm in the former work and ranged between 7.3 and 9.5 atm in the latter; an average P5 of 8.4 atm was used in simulating Nancy data. Under relatively lower-pressure conditions, the model agreement with the data is excellent, and the stoichiometric mixture in the Nancy experiments is represented very well too; on the other hand, the ignition delay times for the rich mixture are slightly underpredicted and those of the lean mixture are overpredicted by about a factor of 2 at higher temperatures.

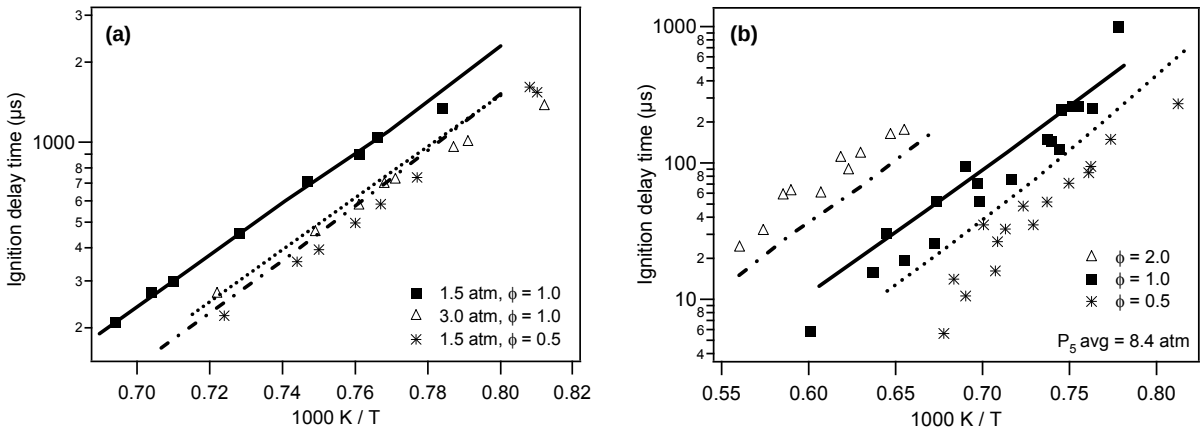

Fig. 16. Cyclohexane shock tube ignition delay times; lines represent simulations and symbols experiments taken from literature [8] and [10].

Ignition delay time sensitivity analyses were performed using our updated mechanism by multiplying and dividing the rate constant by a factor of 2 and recording the resulting ignition delay time (Fig. 17). Three temperatures were chosen in order to accentuate the important reactions for each temperature regime. Figure 17a represents the important reactions for rich and stoichiometric mixtures in air at 750 K, while Fig. 17b represents those for stoichiometric mixtures (in air at 1150 K and diluted in argon at 1500 K), as in the RCM and shock tube experiments. It can be observed quickly in Fig. 17a that the equivalence ratio (varying O_2 concentration) does not have an important effect on sensitivity, and in both figures that temperature has a significant influence on the sensitive reactions. At 750 K, we observe mostly low- and intermediate temperature chemistry affecting the overall reactivity of the system. At this temperature, part of the cy-C_6H_{11} radicals add to molecular oxygen to yield cy-$C_6H_{11}OO$ and the rest oxidizes to cy-C_6H_{10}. The latter pathway has an inhibiting effect for yielding a stable molecule and relatively stable radical HO_2, while the former pathway leads eventually to formation of OH radicals and ketohydroperoxides by decomposition of the OOQOOH and hence has an important promoting effect. Metathesis reactions by OH and HO_2 also have small promoting effects by producing cy-C_6H_{11} radicals. On the other hand, at 1150 K, the H-abstraction reaction by HO_2 has the most important promoting effect, followed by the chain-branching $H+O_2 \leftrightarrows O+OH$. Note that the sensitivity coefficient of this chain-branching reaction is divided by 2 in the plot (Fig. 17b) in order to show the relative importance of other reactions. Ring opening of the cy-C_6H_{11} radical to the 1-hexenyl radical eventually yields 1,3-butadiene and 1-hexene and therefore competes with more reactive pathways, which gives it an overall inhibiting effect. At a higher temperature of 1500 K, the highest sensitivity is observed to $H+O_2 \leftrightarrows O+OH$, and the metathesis reaction by H-atom has an inhibiting effect, given the competition between these. Another competing reaction for H consumption is the recombination with resonantly stabilized allyl radicals yielding stable propene.

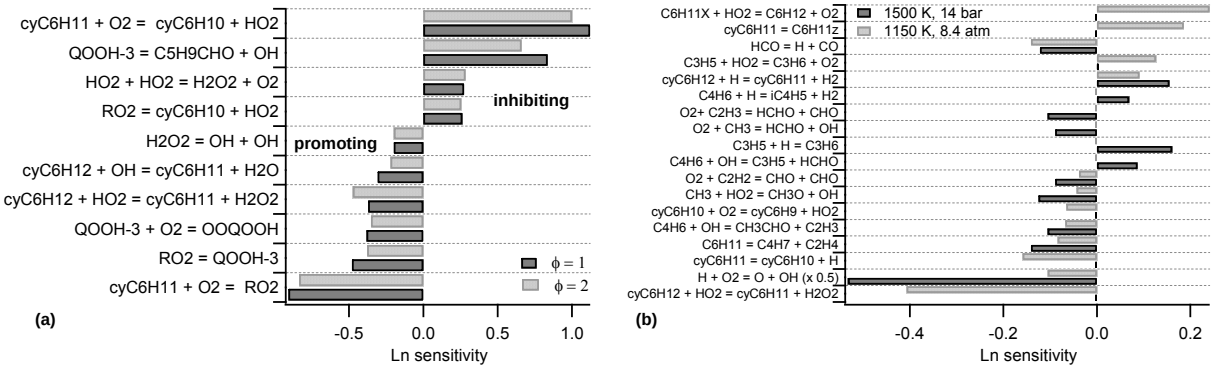

Fig. 17. Sensitivity analysis under (a) RCM conditions: 750 K and 12.5 bar for ϕ = 2 and ϕ = 1 mixtures in air, and (b) ST conditions: 1150 K and 14 bar for ϕ = 1 in air and 1550 K and 8.4 atm for ϕ = 1 diluted in Ar.

As these analyses highlight, low temperature reactions such as first and second additions to oxygen, $RO_2 \leftrightarrows QOOH$ isomerizations, and QOOH decompositions are very sensitive in both the jet-stirred

experiments presented in this work and RCM conditions. Uncertainties related to these may therefore result in rather poor agreement, such as the very high conversion of cy-$C_6H_{11}OO$ to QOOH-3 resulting in overprediction of 5-hexenal and underprediction of 1,2- and 1,4-epoxides, formation of which also depends on the branching ratio between second O_2 additions. As far as the RCM simulations are concerned, in Fig. 17-a QOOH-3+O_2⇆OOQOOH and QOOH-3 → 5-hexenal + OH are sensitive reactions with similar but inverse sign sensitivity coefficients. It is also to be noted that, generally speaking, the lumping procedure employed in the secondary mechanism, such as the globalized decomposition of the ketohydroperoxides, results in some loss of information.

7. Conclusions

Oxidation experiments on cyclohexane were carried out in a jet-stirred reactor for lean (ϕ = 0.5), stoichiometric, and rich (ϕ = 2.0) mixtures of cyclohexane/O_2 with a fuel mole fraction of 0.00667 by varying O2 concentration, at quasi-atmospheric pressure, between 500 and 1100 K and at a residence time of 2 s. Laminar burning velocity of mixtures of cyclohexane in air were measured in a flat flame laminar burner at unburned gas temperatures of 298, 358, and 398 K and 1 atm. A detailed JSR product analysis was carried out using three gas chromatographs. A total of 34 compounds were identified. Among those with the same skeleton as the reactant, epoxycyclohexanes and cyclohexene were formed at both low and high temperatures.

Cyclohexane exhibits very high reactivity at low temperatures and important NTC behavior under studied conditions for ϕ = 0.5 and 1.0; almost no low-temperature reactivity was observed for the rich mixture. The laminar flame speed peak values were measured as 40 cm/s at Ti = 298 K, 52.9 cm/s at 358 K, and 63.1 cm/s at 398 K, at an equivalence ratio of ϕ = 1.1. An updated detailed chemical kinetic model including low-temperature pathways was used to simulate the present experiments as well as some literature data involving shock tube, RCM, and laminar flame speed experiments. Cyclohexane follows a low-temperature reaction pathway very similar to that of n-alkanes; RO_2⇆QOOH isomerization and QOOH decomposition to cyclic ethers are therefore of crucial importance for the whole temperature range considered in this study. In the literature, there are disagreements in the computed values for the latter set of reactions. Further insight into this matter would be very beneficial not only in cyclohexane modeling but also for the development of kinetic mechanisms for larger alkylic naphthenes.

The chemical kinetic mechanism and thermodynamic and transport properties of the species are provided. Jet-stirred reactor experiments by El-Bakali et al. [15] and RCM ignition delay times by Vranckx et al. [12] were simulated with the present mechanism. The present experimental data were also simulated with Sirjean et al. [28] and Silke et al. [25] mechanisms, and these are provided as Supplementary material.

Acknowledgments

The authors thank Dr. Stijn Vranckx and Professor Ravi X. Fernandez for sharing their RCM experimental results. This study has been supported by the ERC Advanced Research Grant "Clean—ICE".

References

[1] W.J. Pitz, C.J. Mueller, Prog. Energy Combust. Sci., 37 (2011), pp. 330–350
[2] A.P. Zeelenberg, H.W. DeBruijn, Combust. Flame, 9 (1965), pp. 281–295
[3] B.H. Bonner, C.F.H. Tipper, Combust. Flame, 9 (1965), pp. 317–327
[4] S.E. Klai, F. Baronnet, J. Chim. Phys., 90 (10) (1993), pp. 1929–1950
[5] S.E. Klai, F. Baronnet, J. Chim. Phys., 90 (10) (1993), pp. 1951–1998
[6] S.K. Gulati, R.W. Walker, J. Chem. Soc., Faraday Trans., 2 (85) (1989), pp. 1799–1812
[7] S.M. Handford-Styring, R.W. Walker, Phys. Chem. Chem. Phys., 3 (2001), pp. 2043–2053
[8] Z. Hong, K.-Y. Lam, D.F. Davidson, R.K. Hanson, Combust. Flame, 158 (2011), pp. 1456–1468
[9] S.M. Daley, A.M. Berkowitz, M.A. Oehlschlaeger, Int. J. Chem. Kinet., 40 (2008), pp. 624–634
[10] B. Sirjean, F. Buda, H. Hakka, P.A. Glaude, R. Fournet, V. Warth, F. Battin-Leclerc, M. Ruiz-Lopez, Proc. Combust. Inst., 31 (2007), pp. 277–284
[11] O. Lemaire, M. Ribaucour, M. Carlier, R. Minetti, Combust. Flame, 127 (2001), pp. 1971–1980
[12] S. Vranckx, C. Lee, H.K. Chakravarty, R.X. Fernandes, Proc. Combust. Inst., 34 (2012), pp. 377–384
[13] Z. Wang, Z. Cheng, W. Yuan, J. Cai, L. Zhang, F. Zhang, F. Qi, J. Wang, Combust. Flame, 159 (2012), pp. 2243–2253
[14] D. Voisin, A. Marchal, M. Reuillon, J.-C. Boettner, Combust. Sci. Technol., 138 (1998), pp. 137–158
[15] A. El-Bakali, M. Braun-Unkhoff, P. Dagaut, P. Frank, M. Cathonnet, Proc. Combust. Inst., 28 (2000), pp. 1631–1638
[16] F. Wu, A.P. Kelley, C.K. Law, Combust. Flame, 159 (2012), pp. 1417–1425
[17] S.G. Davis, C.K. Law, Combust. Sci. Technol., 140 (1998), pp. 427–449
[18] C. Ji, E. Dames, B. Sirjean, H. Wang, F.N. Egolfopoulos, Proc. Combust. Inst., 33 (2011), pp. 971–978
[19] M.E. Law, P.R. Westmoreland, T.A. Cool, J. Wang, N. Hansen, C.A. Taatjes, T. Kasper, Proc. Combust. Inst., 31 (2007), pp. 565–573
[20] C.S. McEnally, L.D. Pfefferle, Combust. Flame, 136 (2004), pp. 155–167
[21] A. Ciajolo, A. Tregrossi, M. Mallardo, T. Faravelli, E. Ranzi, Proc. Combust. Inst., 32 (2009), pp. 585–591
[22] W. Li, M.E. Law, P.R. Westmoreland, T. Kasper, N. Hansen, K. Kohse-Höinghaus, Combust. Flame, 158 (2011), pp. 2077–2089
[23] Y. Yang, A.L. Boehman, Proc. Combust. Inst., 32 (2009), pp. 419–426
[24] S. Granata, T. Faravelli, E. Ranzi, Combust. Flame, 132 (2003), pp. 533–544
[25] E.J. Silke, W.J. Pitz, C.K. Westbrook, M. Ribaucour, J. Phys. Chem. A, 111 (2007), pp. 3761–3775

[26] H. Wang, E. Dames, B. Sirjean, D.A. Sheen, R. Tangko, A. Violi, J.Y.W. Lai, F.N. Egolfopoulos, D.F. Davidson, R.K. Hanson, C.T. Bowman, C.K. Law, W. Tsang, N.P. Cernansky, D.L. Miller, R.P. Lindstedt, JetSurF version 2.0, 2010, <http://melchior.usc.edu/JetSurF/JetSurF2.0>.

[27] F. Buda, B. Heyberger, R. Fournet, P.A. Glaude, V. Warth, F. Battin-Leclerc, Energy Fuels, 20 (2006), pp. 1450–1459

[28] B. Sirjean, P.A. Glaude, M.F. Ruiz-Lopez, R. Fournet, J. Phys. Chem. A, 113 (2009), pp. 6924–6935

[29] D. Matras, J. Villermaux, Chem. Eng. Sci., 28 (1973), pp. 129–137

[30] R. David, D. Matras, Can. J. Chem. Eng., 53 (1975), pp. 297–300

[31] P.A. Glaude, O. Herbinet, S. Bax, J. Biet, V. Warth, F. Battin-Leclerc, Combust. Flame, 13 (2010), pp. 296–308

[32] O. Herbinet, F. Battin-Leclerc, S. Bax, H. Le Gall, P.A. Glaude, R. Fournet, Z. Zhou, L. Deng, H. Guo, M. Xieb, F. Qi, Phys. Chem. Chem. Phys., 13 (2011), pp. 296–308

[33] C. Bahrini, O. Herbinet, P.A. Glaude, C. Schoemaecker, C. Fittschen, F. Battin-Leclerc, J. Am. Chem. Soc., 134 (2012), pp. 11944–11947

[34] P. Dagaut, C. Togbé, Fuel, 89 (2010), pp. 280–286

[35] P. Azay, G.M. Côme, Ind. Eng. Chem. Process Des. Dev., 18 (1979), pp. 754–756

[36] P. Azay, P.M. Marquaire, P. Pommier, G. Scacchi, J. Chem. Educ., 58 (1981)

[37] J. Tranchant, Manuel pratique de chromatographie en phase gazeuse, Masson, Paris, France (1995)

[38] P. Dirrenberger, H. Le Gall, R. Bounaceur, O. Herbinet, P.A. Glaude, A.A. Konnov, F. Battin-Leclerc, Energy Fuels, 25 (9) (2011), pp. 3875–3884

[39] F. Gillespie, W.K. Metcalfe, P. Dirrenberger, O. Herbinet, P.A. Glaude, F. Battin-Leclerc, H.J. Curran, Energy, 43 (1) (2012), pp. 140–145

[40] K.J. Bosschaart, L.P.H. de Goey, Combust. Flame, 136 (3) (2004), pp. 261–269

[41] V. Warth, N. Stef, P.A. Glaude, F. Battin-Leclerc, G. Scacchi, G.M. Côme, Combust. Flame, 114 (81) (1998), p. 102

[42] F. Buda, R. Bounaceur, V. Warth, P.A. Glaude, R. Fournet, F. Battin-Leclerc, Combust. Flame, 142 (2005), pp. 170–186

[43] D.L. Baulch, C.J. Cobos, R.A. Cox, P. Franck, G.D. Hayman, T. Just, J.A. Kerr, T.P. Murrells, M.J. Pilling, J. Troe, R.W. Walker, J. Warnatz, Combust. Flame, 98 (1994), pp. 59–79

[44] D.L. Baulch, C.T. Bowman, C.J. Cobos, R.A. Cox, T. Just, M.J. Pilling, D. Stocker, J. Troe, W. Tsang, R.W. Walker, J. Warnatz, J. Phys. Chem. Ref. Data, 34 (2005), pp. 757–1397

[45] W. Tsang, R.F. Hampson, J. Phys. Chem. Ref. Data, 15 (1986), pp. 1087–1279

[46] S. Touchard, R. Fournet, P.A. Glaude, V. Warth, F. Battin-Leclerc, G. Vanhove, M. Ribaucour, R. Minetti, Proc. Combust. Inst., 30 (2005), pp. 1037–1081

[47] R. Bounaceur, V. Warth, B. Sirjean, P.A. Glaude, R. Fournet, F. Battin-Leclerc, Proc. Combust. Inst., 32 (2009), pp. 387–394

[48] J. Biet, M.H. Hakka, V. Warth, P.A. Glaude, F. Battin-Leclerc, Energy Fuels, 22 (2008), pp. 2258–2269

[49] C. Muller, V. Michel, G. Scacchi, G.M. Côme, J. Chim. Phys., 92 (1995), pp. 1154–1178

[50] S.W Benson, Thermochemical Kinetics, Wiley, New York (1976), pp. 19–78

[51] B. Sirjean, P.A. Glaude, M. Ruiz-Lopez, R. Fournet, J. Phys. Chem. A, 112 (2008), pp. 11598–11610

[52] H. Wang, M. Frenklach, Combust. Flame, 96 (1994), pp. 163–170

[53] X. You, H. Wang, E. Goos, C.-J. Sung, S.J. Klippenstein, J. Phys. Chem. A, 111 (2007), pp. 4031–4042

[54] V. Vasudevan, D.F. Davidson, R.K. Hanson, Int. J. Chem. Kinet., 37 (2005), pp. 98–109

[55] J. Troe, Combust. Flame, 158 (2011), pp. 594–601

[56] R. Sivaramakrishnan, J.V. Michael, Combust. Flame, 156 (2009), pp. 1126–1134

[57] N. Cohen, Int. J. Chem. Kinet., 14 (1982), pp. 1339–1362

[58] B. Heyberger, N. Belmekki, V. Conraud, P.A. Glaude, R. Fournet, F. Battin-Leclerc, Int. J. Chem. Kinet., 34 (2002), pp. 666–677
[59] C. Cavallotti, R. Rota, T. Faravelli, E. Ranzi, Proc. Combust. Inst., 31 (2007), pp. 201–209
[60] S.M. Villano, L.K. Huynh, H.-H. Carstensen, A.M. Dean, J. Phys. Chem. A, 116 (2012), pp. 5068–5089
[61] A. Miyoshi, J. Phys. Chem. A, 115 (2011), pp. 3301–3325
[62] M. Cord, B. Sirjean, R. Fournet, A. Tomlin, M. Ruiz-Lopez, F. Battin-Leclerc, J. Phys. Chem. A, 116 (2012), pp. 6142–6158
[63] C.D. Wijaya, R. Sumathi, W.H. Green, J. Phys. Chem. A, 107 (2003), pp. 4908–4920
[64] Y. Yang, A.L. Boehman, J.M. Simmie, Combust. Flame, 157 (2010), pp. 2357–2368
[65] A.M. Knepp, G. Meloni, L.E. Jusinski, C.A. Taatjes, C. Cavallotti, S.J. Klippenstein, Phys. Chem. Chem. Phys., 9 (2007), pp. 4315–4331
[66] B. Husson, O. Herbinet, P.A. Glaude, S.S. Ahmed, F. Battin-Leclerc, J. Phys. Chem. A, 116 (2012), pp. 5100–5111
[67] A.T. Droege, F.P. Tully, J. Phys. Chem., 91 (1987), pp. 1222–1225
[68] R. Atkinson, Atm. Chem. Phys., 3 (2003), pp. 2233–2307